BMC Biology

RESEARCH ARTICLE

Open Access

The m6A writer KIAA1429 regulates photoaging progression via MFAP4-dependent collagen synthesis

Yuanyuan Liu[1,2], Jian Li[3], Chenhui Wang[4†], Jiangbo Li[4], Kai Luo[5], Kang Tao[3], Yuan Tian[3], Xiang Song[4], Zhifang Zhai[3], Yuandong Tao[6], Jia You[5], Lihua Wu[5], Wenqian Li[7], Yuanyuan Jiao[8], Rongya Yang[2*] and Mingwang Zhang[3*]

Abstract

Background N6-Methyladenosine (m^6A) methylation, a common form of RNA modification, play an important role in the pathogenesis of various diseases and in the ontogeny of organisms. Nevertheless, the precise function of m^6A methylation in photoaging remains unknown.

Objectives This study aims to investigate the biological role and underlying mechanism of m^6A methylation in photoaging.

Methods m^6A dot blot, Real-time quantitative PCR (RT-qPCR), western blot and immunohistochemical (IHC) assays were employed to detect the m^6A level and specific m^6A methylase in ultraviolet ray (UVR)-induced photoaging tissue. The profile of m^6A-tagged mRNA was identified by methylated RNA immunoprecipitation sequencing (MeRIP-seq) and RNA-seq analysis. Finally, we investigated the regulatory mechanism of KIAA1429 by MeRIP-qPCR, RNA knockdown and immunofluorescence assay.

Results m^6A levels were increased in photoaging and were closely associated with the upregulation of KIAA1429 expression. 1331 differentially m^6A methylated genes were identified in the UVR group compared with the control group, of which 1192 (90%) were hypermethylated. Gene ontology analysis showed that genes with m^6A hypermethylation and mRNA downregulation were mainly involved in extracellular matrix metabolism and collagen metabolism-related processes. Furthermore, KIAA1429 knockdown abolished the downregulation of TGF-bRII and upregulation of MMP1 in UVR-irradiated human dermal fibroblasts (HDFs). Mechanically, we identified MFAP4 as a target of KIAA1429-mediated m^6A modification and KIAA1429 might suppress collagen synthesis through an m^6A-MFAP4-mediated process.

†Yuanyuan Liu, Jian Li, Chenhui Wang contributed equally to this work and share first authorship.

†Rongya Yang and Mingwang Zhang contributed equally to this work and share last authorship.

*Correspondence:
Rongya Yang
RongyaYang960@outlook.com
Mingwang Zhang
mingwangzhang56@outlook.com
Full list of author information is available at the end of the article

Conclusions The increased expression of KIAA1429 hinders collagen synthesis during UVR-induced photoaging, suggesting that KIAA1429 represents a potential candidate for targeted therapy to mitigate UVR-driven photoaging.

Keyword Photoaging, N6-methyladenosine (m^6a), KIAA1429, MFAP4

Background

Photoaging, the most significant form of extrinsic skin aging, encompasses a confluence of physical features such as skin laxity, wrinkles, dyspigmentation, telangiectasia, elastosis, xerosis, and coarseness, mainly due to long-term effects of repeated exposure to ultraviolet ray (UVR) [1]. UVR is divided into three components according to wavelength: UVA (320–400 nm), UVB (280–320 nm), and UVC (200–280 nm). UVC is absorbed in the stratosphere and only UVA and UVB exert biological effects on the skin (~95% UVA, ~5% UVB). UVB, with its high energy and short wavelength, penetrates the epidermis and exerts a significant influence on photoaging, while UVA, although less potent, accounts for approximately 95% of the UV radiation that reaches the skin. Both UVA and UVB play a substantial role in photoaging by interfering with signaling pathways involved in the expression of important genes which related to collagen metabolism and extracellular matrix formation [2]. However, whether the expression of these genes is subject to post-transcriptional regulation remains unclear.

The methylation of adenosine at the N6 position (N6-methyladenosine or m^6A) is the most prevalent mRNA modification in eukaryotes, with up to 25% of mRNAs possessing at least one m^6A residue [3]. m^6A levels are dynamically regulated by methyltransferases and demethylases, also known as "writers" and "erasers", respectively. Current research has found that writers mainly consisted of METTL3 and METTL14 and cofactors WTAP, KIAA1429, RBM15, RBM15B, and ZC3H13, while erasers included only FTO and ALKBH5. In addition, a panel of specific RNA-binding proteins, also called "readers", composed of YTHDF1/2/3 and other proteins can recognize m^6A motif and thus affect m^6A function. m^6A modulates several stages of mRNA processing, including RNA splicing, nuclear export, localization, stability and translation. At the cellular and organismal levels, it participates in a vast array of physiological and pathological processes, including pluripotency, carcinogenesis, metabolic disease, autoimmune disease, etc. [4, 5]. A recent study reported that m^6A RNA modification is rapidly activated at DNA damage sites induced by UVR in A375 and U2OS cells, which could promote noncanonical nucleotide excision repair (NER) via recruitment of Pol κ [6]. In addition, Yang et al. [7] demonstrated that METTL14 may act as an emerging epitranscriptomic mechanism to regulate global genome repair (GGR) and suppress UVB damage response in tumorigenesis. However, the extent to which m^6A influences collagen metabolism, a critical player in photoaging, remains unknown.

In this study, we systematically investigated alterations in the m^6A methylation and mRNA expression profiles in the skin tissue of photodamaged mice by using methylated RNA immunoprecipitation (MeRIP)-seq and RNA-seq. A large number of dysregulated m^6A-modified mRNAs were identified during photoaging processes. Moreover, we demonstrated that KIAA1429 promotes collagen metabolism by regulating m^6A mRNA methylation-mediated MFAP4 expression and suppressing UVR-induced skin photoaging. Our research, for the first time, provides a novel epigenetic regulatory mechanism for photoaging.

Results

Global m^6A levels were increased in UVR-induced photoaging

To investigate the alteration of m^6A modification levels during photoaging, we constructed a murine model, as described in the Methods section. After 12 weeks, the UVR group exhibited symptoms of skin aging, including dryness, scaliness, wrinkling, dilated capillaries, and a leathery appearance, compared with the control group. Hematoxylin–eosin (HE) staining displayed hyperkeratosis of the epidermis with irregular thickening, decreased collagen fiber density, angiotelectasis, and inflammatory cell infiltration in the dermis (Fig. 1A-C). Furthermore, ELISA demonstrated a significant decrease in the activity of superoxide dismutase (SOD) and the content of hydroxyproline (Hyp), along with an increase in the level of malondialdehyde (MDA) (Fig. 1D, E). Western blot analysis of transforming growth factor-beta receptor 2 (TGF-βRII) expression revealed a significant decrease, while matrix metalloproteinase 1 (MMP-1) synthesis was elevated in UVR-induced photoaged skin compared to the control (Fig. 1F). Collectively, these findings indicate the successful construction of a murine model of skin photoaging.

We then investigated alterations in the levels of m6A modification in mRNA of UVR-induced photoaged skin. Two groups of mouse skin tissues were collected and subjected to total mRNA extraction. RNA dot blotting was performed to analyze the dynamic changes in global m6A levels, and significantly increased m6A levels were

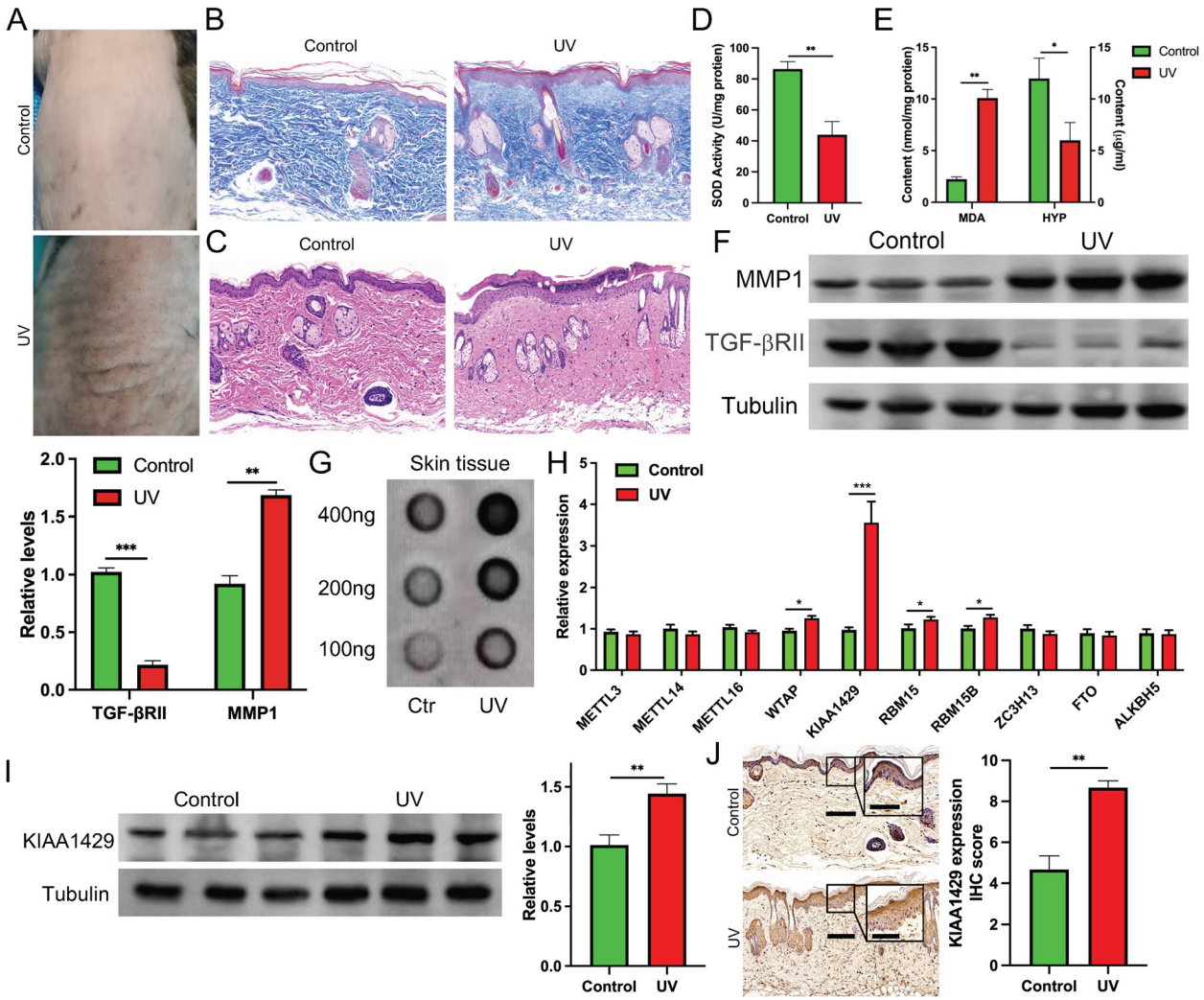

Fig. 1 Global m^{6}A levels and methyltransferases KIAA1429 expression were significantly upregulated in UVR-induced photoaged skin. **A** The clinical manifestations of dorsal skin in the control and UVR group. **B** HE staining of skin in each group. Magnification: 100×. **C** Masson stain of skin in each group. Magnification: 100×. **D** SOD levels in each group by ELISA ($n=7$). **E** MDA and Hyp levels in each by ELISA ($n=7$). **F** Protein expression of TGF-bRII and MMP1 were evaluated by western blot ($n=3$). **G** The m^{6}A levels of total mRNA were determined by m^{6}A dot blot in both groups. **H** The mRNA expression of METTL3, METTL14, METTL16, WTAP, KIAA1429, RBM15, RBM15B, ZC3H13, FTO and ALKBH5 were indicated by RT-qPCR ($n=7$). **I** Protein level of KIAA1429 was detected by western blot in each group ($n=3$). **J** IHC staining for KIAA1429 protein from skin tissue in each group ($n=7$). Scale bar is 100 μm and 50 μm (magnified). All data were presented as mean ± standard deviation (SD) of three independent experiments. $^{*}p<0.05$, $^{**}p<0.01$, $^{***}p<0.001$

observed in the UVR group compared with the control (Fig. 1G).

Previous studies have demonstrated that the dynamic level of m^{6}A modification is regulated by methyltransferases and demethylases [8]. We analyzed the expression of m6A methyltransferases METTL3, METTL14, METTL16, WTAP, KIAA1429, RBM15, RBM15B, ZC3H13, and m6A demethylases FTO, ALKBH5 in photoaged skin and control using RT-qPCR. Among them, KIAA1429 revealed the most significant upregulation and was consistent with the increase in m6A abundance during photoaging (Fig. 1H). The protein level of KIAA1429 determined by Western blotting was also significantly increased in skin tissue (Fig. 1I). Additionally, we discovered strongly higher positive scores in photoaging tissue based on IHC staining (Fig. 1J). Collectively, these data reveal that UVR-induced photoaging enhances KIAA1429 expression and might consequently upregulate m6A levels in the skin.

Analysis of m^{6}A methylation map in photoaging mice and controls

To characterize the transcript-specific m^{6}A changes evoked by photoaging, we analyzed the m^{6}A-methylated mRNA expression profile in the skin tissues of photoaging mice and controls using MeRIP-seq. Correlation heatmap analysis revealed that both UVR and control samples had good biological reproducibility among the three replicates of each group (Fig. 2A). GGACU sequence was the highest enriched m^{6}A motif in both groups consistent with previous studies [9] (Fig. 2B). A total of 24,969 and 18,020 m^{6}A peaks from 10,652 to 8,766 m^{6}A-modified transcripts in UVR and control groups, respectively. For m^{6}A-regulated genes, 2310 new

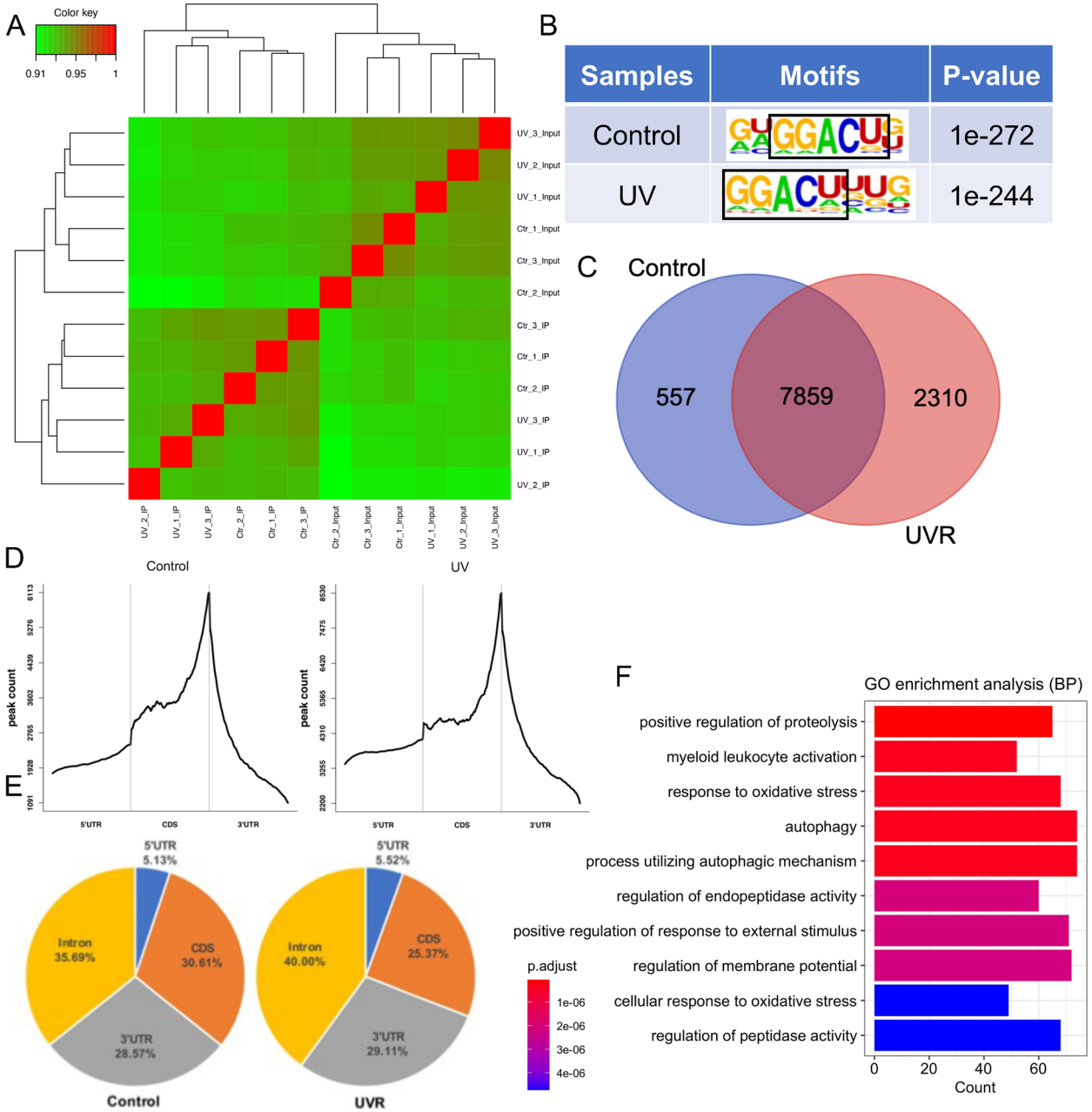

Fig. 2 Features of mRNA m^{6}A methylation map in skin tissue with or without UVR irradiation. **A** Correlation heatmap analysis of each sample. **B** The enriched motif of m^{6}A peaks was identified by HOMER in each group. **C** Venn diagrams displaying the differences and overlap of m^{6}A-containing genes in control and photoaged skin, respectively. **D** The distribution of m^{6}A peaks across the mRNA regions. **E** Pie charts showing the proportion of m^{6}A peaks in different mRNA regions in each group. **F** Biological processes of 2310 photoaging-unique m^{6}A-modified genes

m^{6}A peaks-containing genes and 557 genes disappearing peaks were identified in the UVR sample, while the other 7859 genes were found in both groups (Fig. 2C), indicating the significant alteration of the m^{6}A modification expression profile during photoaging. We further analyzed the total m^{6}A peak distribution in each functional region of the genes. Similar patterns of the total m^{6}A distribution in two group samples were observed, showing that m^{6}A peaks were mainly abundant in the vicinity of stop codons (Fig. 2D, E). Furthermore, we performed the GO enrichment analysis of the 2310 unique peaks-containing genes in the UVR sample. The results showed that they were highly enriched in some biological processes, such as response to oxidative stress and autophagy (Fig. 2F), both of which have been previously shown to be strongly associated with the development of photoaging [10, 11].

DMMGs are involved in collagen metabolism of the UVR-induced photoaging

To further clarify the effect of transcript-specific m6A changes on the corresponding mRNA expression, we first identified 1331 DMMGs in the UVR group compared with control samples, using the screening criteria of $|FC| \geq 2$ and p-value < 0.05. Consistent with the global elevation of m^{6}A methylation in photoaging, 1192 (90%) mRNAs were significantly hypermethylated, and only 139 mRNAs (10%) were significantly hypomethylated in the UVR tissues compared with controls (Fig. 3A and Additional file 1: Table S1). The top five hypermethylated genes and the top five hypomethylated genes were selected to determine the enrichment of m^{6}A using MeRIP-qPCR. The results were highly consistent with the MeRIP-seq data when normalized with IgG negative control for each sample (Fig. 3B). Subsequently, we analyzed the expression profile of mRNA in two groups using RNA-seq. Compared with the control group, 347 significant DEGs were identified in the UVR group, with 125 upregulated genes and 222 downregulated genes (Fig. 3C, Additional file 2: Table S2). RT-qPCR was performed for the top five upregulated and top five downregulated genes to validate the RNA-seq data. Most of tested genes showed high concordance with the sequencing results (Fig. 3D). Lastly, we conducted a conjoint analysis for DMMGs and DEGs to investigate the correlation between m^{6}A methylation and mRNA abundance according to the criteria of $|FC| \geq 1.25$ and p-value < 0.05. 209 genes showed both significant differences in m^{6}A methylation levels and expression levels, among them,79 hypermethylated genes were upregulated (hyper-up), 98 hypermethylated genes were downregulated (hyper-down), 14 hypomethylated genes were upregulated genes (hypo-up) and 18 hypomethylated genes were downregulated genes (hypo-down) (Fig. 3E). Functional enrichment analysis displayed that hyper-down genes were mainly involved in extracellular matrix metabolism and collagen metabolism-related processes, while other parts of genes were not enriched in pathways associated with photoaging (Fig. 3F, Additional file 3: Figure S1-S3). This suggested that the m^{6}A hyper-methylation could be involved in the photoaging process by downregulating the expression of genes related to extracellular matrix metabolism.

KIAA1429 regulated collagen metabolism in UVR-induced photoaging through m^{6}A

Since collagen metabolism was primarily associated with fibroblasts, we hypothesized that the subpopulation of cells in skin tissue in which m^{6}A modification resulted in the downregulation of genes related to collagen metabolism was HDFs. In order to substantiate this claim, we first examined the m^{6}A levels in UVR-irradiated HDFs cells, as well as the mRNA and protein levels of KIAA1429. The results were indicative of a robust congruence with those observed in photoaged skin (Fig. 4A - C).

To characterize the role of KIAA1429 in the photoaging process, we constructed KIAA1429 knockdown HDFs by transfection of the KIAA1429-specific small interfering RNAs (siRNA). Transcript levels were examined to confirm the transfection effect (Fig. 4D). Notably, the results showed that KIAA1429 knockdown cells manifested a significant reduction in the m^{6}A levels relative to wild-type cells in response to UVR-irradiation (Fig. 4E). Moreover, UVR-induced downregulation of TGF-bRII and upregulation of MMP1 was rescued in si-KIAA1429 HDFs cells (Fig. 4F). Immunofluorescence assay showed that KIAA1429 knockdown increased the signal of COL1a2 on the cells by using an anti-COL1a2 antibody (Fig. 4G). Collectively, these findings demonstrated that the activity of KIAA1429 is increased and might regulate collagen metabolism through m^{6}A modification in UVR-induced photoaging.

KIAA1429 suppresses collagen production through an m^{6}A-MFAP4-mediated manner in UVR-irradiated HDFs

According to the above results, we speculated that KIAA1429, through an m^{6}A-dependent mechanism, could regulate the metabolism of TGFβ and collagen via one or more genes in photoaging. We screened the hyper-down portion of the gene and then found MFAP4 which has been reported to be both down-regulated in photoaging and could regulate TGFβ/Smad pathway activity [12, 13]. Firstly, to identify whether the m^{6}A modification of MFAP4 was mediated by KIAA1429, we conducted the MeRIP-qPCR

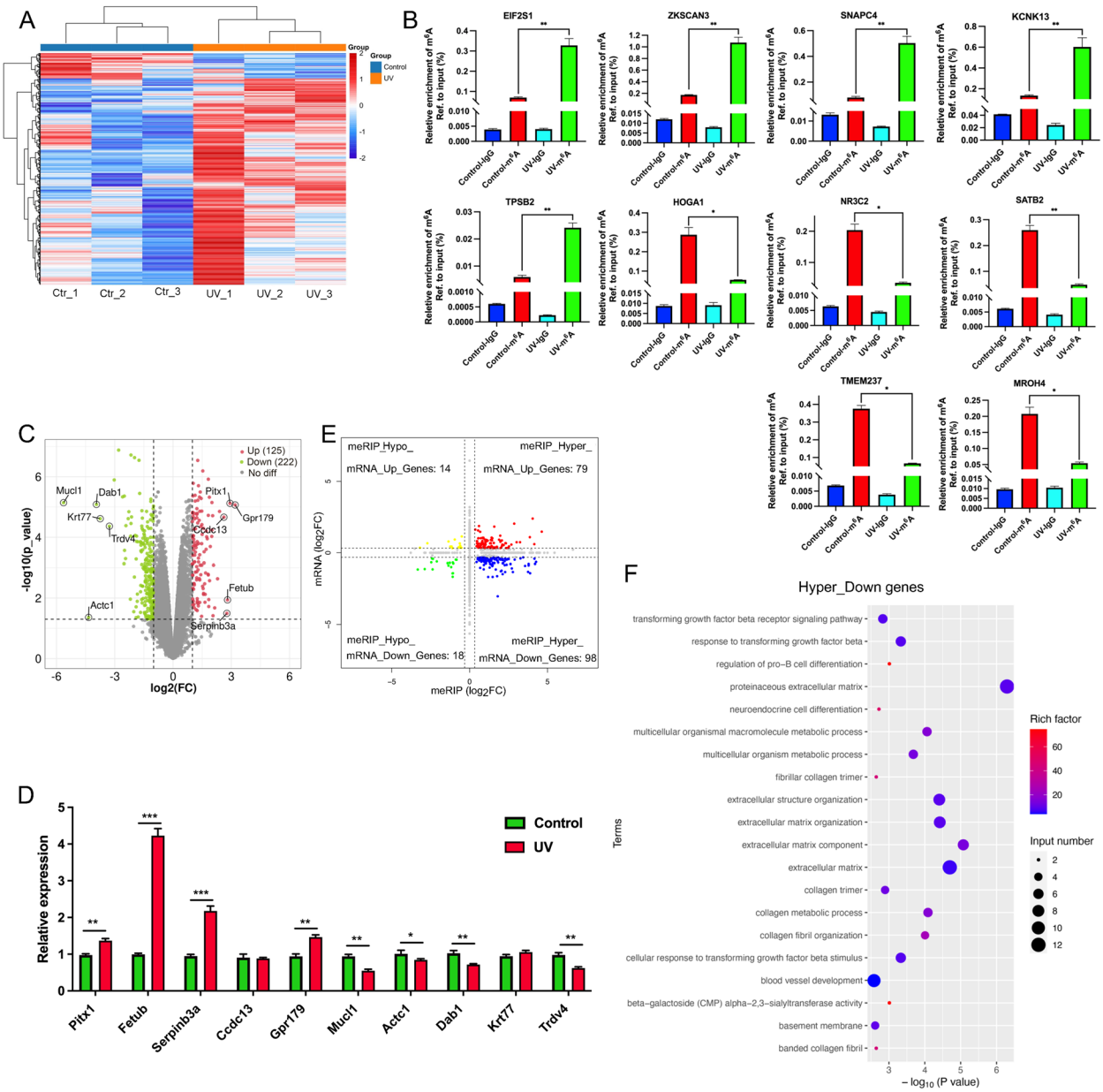

Fig. 3 DMMGs were involved in collagen metabolism in UV-induced photoaging. **A** Hierarchical cluster analysis of DMMGs between the control group and photoaged group. **B** MeRIP-qPCR analysis validated the m^{6}A levels of the top 5 hyper-methylation and 5 hypo-methylation genes ($n = 7$). m^{6}A-IP/input and IgG-IP/input were used to calculate the enrichment of m^{6}A in each group. **C** Volcano plot of DEGs between the two groups. **D** RT-qPCR validated the top DEGs between the two groups ($n = 7$). **E** Venn diagram of genes with a significant change in both the m^{6}A methylation and mRNA expression levels. **F** The top 20 GO biological processes enrichments of genes from the hyper-down part. All data were presented as mean ± SD of three independent experiments. $^{*}p < 0.05$, $^{**}p < 0.01$, $^{***}p < 0.001$

assay to evaluate the m^{6}A levels of MFAP4 in KIAA1429 knockdown group and control group with or without UVR irradiation. Indeed, we found that extrinsically UV irradiation significantly increased the m^{6}A enrichment across the transcript of MFAP4 in HDFs, while a significant reduction of m^{6}A levels in MFAP4 mRNA following KIAA1429 silencing (Fig. 5A). Next, we investigated the mRNA and protein expression of MFAP4 in si-KIAA1429 HDFs cells. We observed that UVR-induced downregulation of MFAP4 was rescued in KIAA1429 knockdown cells (Fig. 5B and C), which indicated that KIAA1429 participated in the UVR-induced decrease of MFAP4 in HDFs. Finally, we further investigated the role of MFAP4 in KIAA1429-regulated collagen metabolism in HDF cells. Transfection with

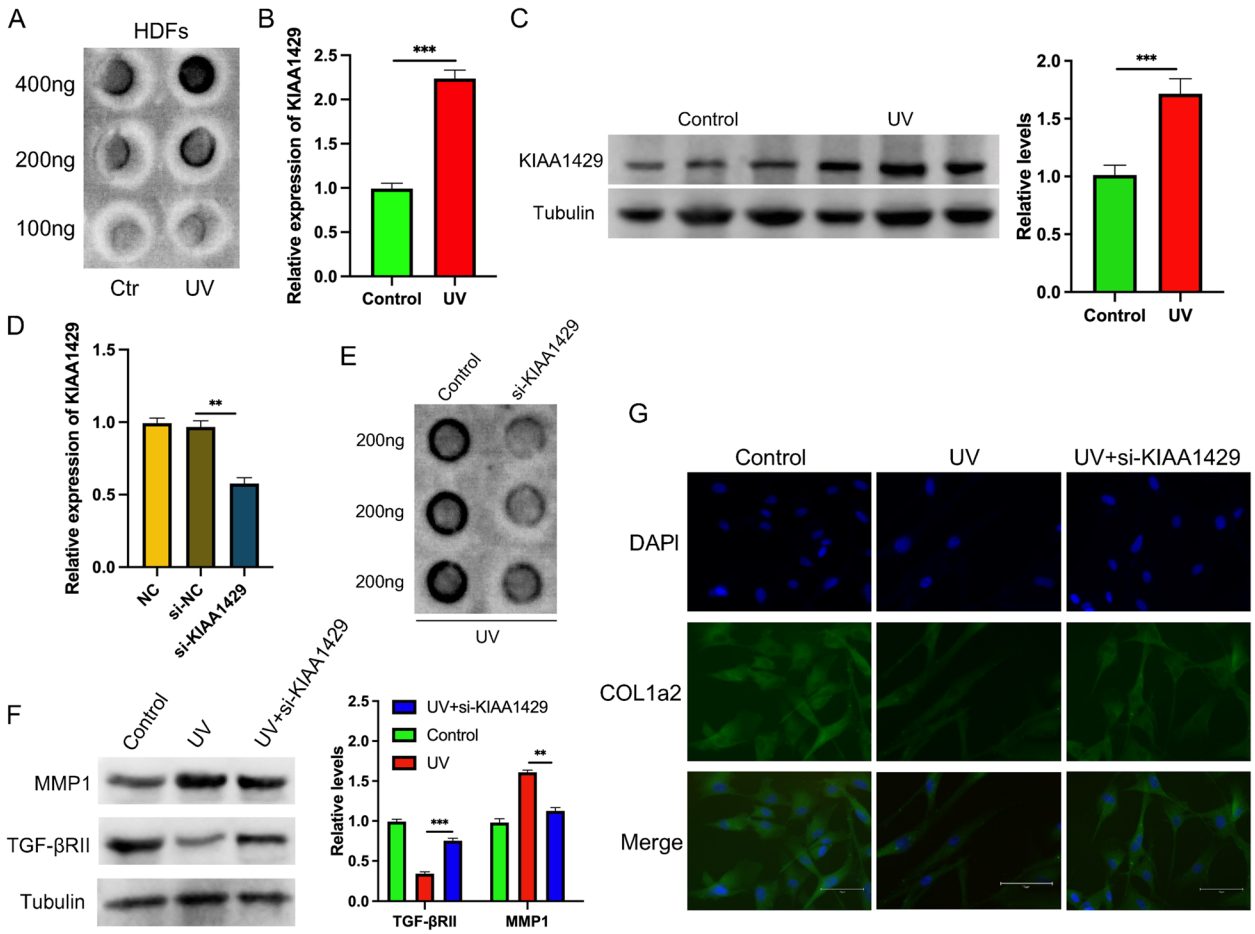

Fig. 4 KIAA1429 regulated collagen synthesis in UVR-irradiated HDFs. **A** The m^{6}A levels of total mRNA in control and UVR-irradiated HDFs were detected using m^{6}A dot blot. **B** mRNA expression of KIAA1429 was identified by RT-qPCR between the two groups ($n=7$). **C** The protein level of KIAA1429 in two groups was detected using western blot ($n=3$). **D** RT-qPCR detects the effect on knockdown of KIAA1429 expression by siRNA in the HDFs cells ($n=7$). **E** The m^{6}A levels content of mRNA were identified by m^{6}A dot blot in UVR-irradiated HDFs with or without KIAA1429 knockdown. **F** The protein levels of TGF-bRII and MMP1in control and UVR-irradiated HDFs transfected with or without si-KIAA1429 were measured using western blot ($n=3$). **G** Immunofluorescence staining was performed with anti-COL1A2 in each group. Nuclear staining (DAPI) and merged images are also shown in the diagram. Scale bars = 75 μm. All data were presented as mean ± SD of three independent experiments. $^{**}p<0.01$, $^{***}p<0.001$

si-MFAP4 antagonized the downregulation of MMP1 and upregulation of TGF-bRII in KIAA1429 knockdown HDFs cells during UVR-induced photoaging (Fig. 5D). In addition, Immunofluorescence analysis also confirmed that MFAP4 knockdown reduced the signal of colocalization of COL1A2 and MFAP4 in KIAA1429 knockdown HDFs cells after UVR irradiation (Fig. 5E). These findings suggested that KIAA1429 repressed collagen generation through an m^{6}A-MFAP4-dependent pathway.

Discussion

Leveraging advancements in next-generation sequencing technology, various epigenetic mechanisms, including DNA methylation, histone acetylation, and mRNA methylation, have been confirmed as significant contributors to numerous physiological and pathological processes, including intrinsic aging [14]. Nevertheless, the precise role of m6A modification in collagen metabolism during extrinsic aging (photoaging) and the underlying regulatory mechanisms of m6A effectors remain poorly understood. In this study, we demonstrate a significant increase in global m6A levels in UVR-induced photoaging models compared to controls, primarily attributed to the upregulation of KIAA1429. Our combined analysis of MeRIP-seq, RNA-seq, and GO analysis reveals that differentially expressed genes (DEGs) involved in collagen metabolism and extracellular processes are significantly regulated by m6A during photoaging. Notably, MFAP4, a

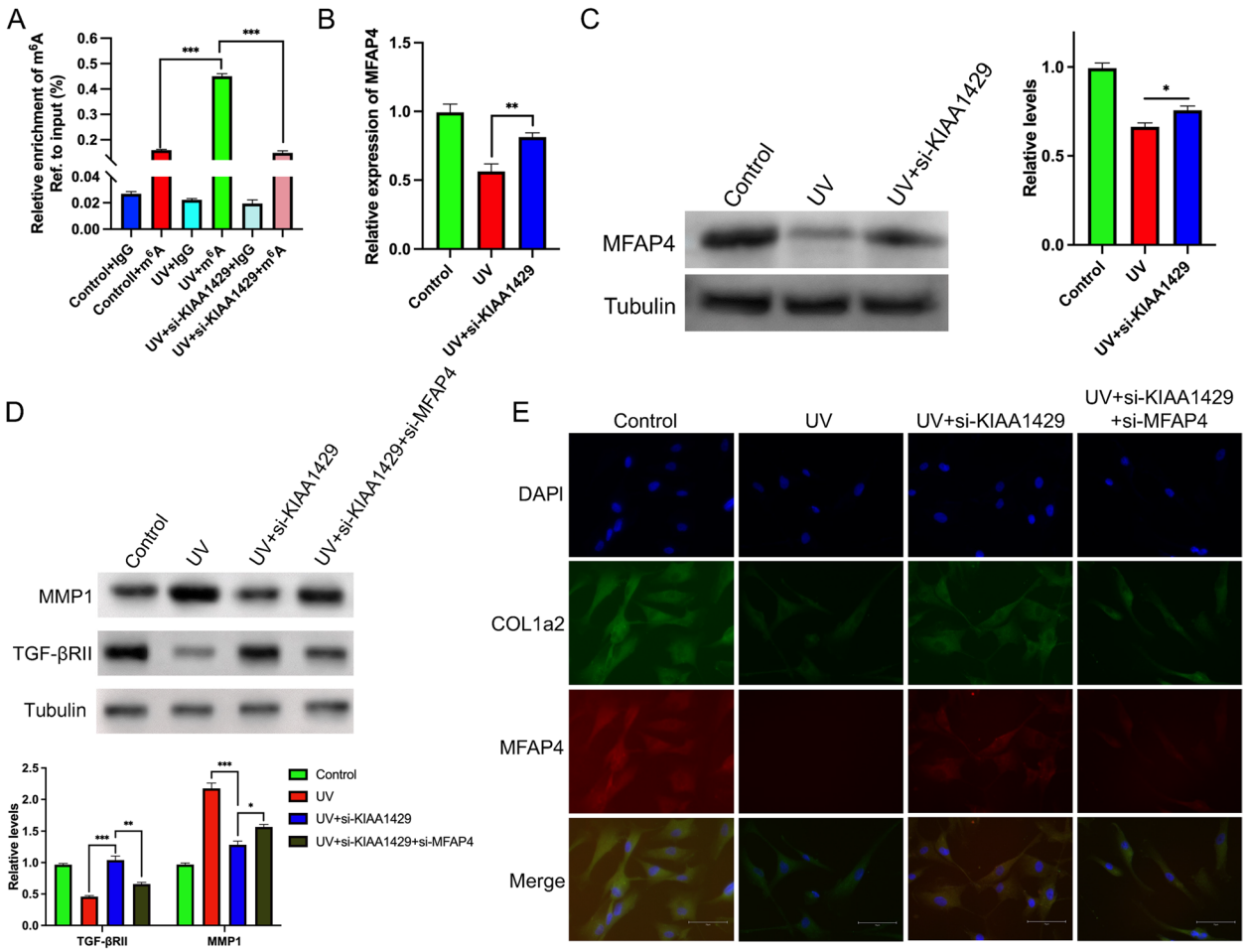

Fig. 5 KIAA1429 repressed collagen synthesis in UVR-irradiated HDFs via m^{6}A-MFAP4-mediated manner **A** MeRIP-qPCR was applied to assess the m^{6}A modification of MFAP4 in control and UVR-irradiated HDFs transfected with or without si-KIAA1429. m^{6}A-IP/input and IgG-IP/input were used to calculate the enrichment of m^{6}A in each group ($n=7$). **B** RT-qPCR detected the mRNA expression of MFAP4 in each group ($n=7$). **C** The protein level of MFAP4 was identified using western blot in each group ($n=3$). **D** Western blot of the expression of TGF-bRII and MMP1 in each group ($n=3$). **E** Immunofluorescence assay of the colocalization of COL1a2 with MFAP4 in each group. Nuclear staining (DAPI) and merged images are also shown in the diagram. Scale bars = 75 μm. All data were presented as mean ± SD of three independent experiments. $^{*}p<0.05$, $^{**}p<0.01$, $^{***}p<0.001$

key protein in elastic fiber formation and collagen metabolism, is identified as m6A methylated and regulated by KIAA1429. Furthermore, the knockdown of KIAA1429 promotes collagen production in UVR-induced photoaging, an effect attenuated by the depletion of MFAP4.

Initially, we showed that global m^{6}A levels were significantly increased in UVR-induced photoaged mice skin and UVR-irradiated HDFs cells. The results of the cellular fraction are consistent with previous findings reported by Ouyang et al. [15]. However, earlier studies by Xiang and colleagues reported that the m^{6}A level in poly(A)$^+$ RNA was transiently induced and peaked rapidly at 2 min, followed by a gradual decrease after UVC irradiation in U2OS cells [6]. A recent report showed that UVB irradiation decreased the total and poly(A)$^+$ RNA m^{6}A levels in both HaCaT and normal human epidermal keratinocyte (NHEK) cells [7]. It is possible that m^{6}A modification exhibited tissue- and cell-specific regulations [3], since the samples we used were different from other studies. In addition, previous studies have found that different wavelengths of UV light could induce distinct cellular and molecular responses [16], we speculated that this might be also related to the different results in m^{6}A levels.

Cellular m^{6}A modification levels were regulated through the coordinated activity of m^{6}A methylases and demethylases. So, we detected the expression of m^{6}A writers and erasers that have been reported to date

and found that KIAA1429 was the most significantly increased writer using multiple assays, which could explain the elevated m^{6}A levels in UVR-induced photoaging. Meanwhile, we have noted that several other writers and erasers were also significantly changed as presented in Fig. 1H, and some of the changes were consistent with altered m^{6}A levels, which cannot exclude that m^{6}A modifications levels are modulated by other regulators in UVA-induced photoaging. Several studies have reported that m^{6}A-related enzymes including METTL14, METTL3 and FTO participated in the regulation of m^{6}A levels after UV irradiation in different samples, of which different biological effects have been demonstrated [6, 7, 15]. Therefore, it remains to be elucidated of other differentially expressed writers and erasers from the current study in the future.

KIAA1429, the largest known protein of the methyltransferase complex, has been recognized as an indispensable factor for the entire process of mRNA methylation since 2015 [17]. The m^{6}A modification region by KIAA1429 was enriched in the 3′-UTR and stop codon of RNA sequences [18]. This corroborates, which is consistent with Fig. 2D of this research. Several studies have reported that KIAA1429 mainly acts as an oncogene in a variety of malignancies, as well as multiple non-neoplastic diseases, indicating its versatility [19, 20]. In addition, a recent study found that the expression of KIAA1429 varied in H_2O_2-induced senescence cells, replicative senescence cells and young human embryonic lung fibroblasts, but the investigators did not further explore the mechanism of altered KIAA1429 expression on cell senescence [21]. In this study, we revealed that the expression of KIAA1429 remarkably increased in UVR-induced photoaging model. KIAA1429 knockdown decreased the global m^{6}A levels and m^{6}A enrichment in the MFAP4 transcript. Moreover, KIAA1429 negatively regulated collagen production through inhibition of the MFAP4 transcription. These findings support the critical role of KIAA1429 in regulating photoaging through participating in collagen metabolism. Nonetheless, the specific mechanism of the upregulation of KIAA1429 in photoaging remains enigmatic.

We also observed that MFAP4 expression was significantly reduced in UVR-induced photoaged mouse skin and UVR-irradiated HDFs cells. The result was consistent with previous studies [12, 22]. MFAP4, an extracellular matrix protein, manifests an ability to attach itself to collagen, fibrillins, and tropoelastin, thereby playing a crucial role in microfibril assembly, tropoelastin coacervation, and collagen degradation [12, 23]. Moreover, MFAP4 has been found to promote the activation of the TGF-b pathway, which has a key role in tissue remodeling, and seems to be itself a product of TGF-b-related signaling, thus possibly activating an autocrine circuit in several tissue remodeling-associated diseases, such as fibrosis or cardiovascular disorders [24]. In the present study, we found that knockdown of MFAP4 significantly reduced the expression of TGF-bRII, suppressed the signal of colocalization of COL1A2 and MFAP4, and increased the secretion of MMP1 in UV-irradiated KIAA1429 knockdown HDF cells, suggesting that MFAP4 could participate in photoaging through modulating the TGF-β pathway. However, further experiments, such as loss- and gain- of function assays, are warranted to corroborate this finding.

m^{6}A modifications can modulate gene expression through regulating mRNA stability, mRNA export, mRNA translation, etc. [5]. We showed that KIAA1429 knockdown significantly reduced m^{6}A enrichment in the MFAP4 transcript, and m^{6}A RNA methylation levels negatively regulate MFAP4 mRNA expression, accompanied by a decrease in protein level. However, we did not investigate the specific m^{6}A reader protein that recognizes the m^{6}A-modified locus in MFAP4 and the underlying mechanisms that lead to the alterations in mRNA and protein. It is possible that either the m^{6}A reader affected MFAP4 mRNA stability or other biological processes, necessitating further experimentation, such as crosslinking and immunoprecipitation (CLIP) or RNA pull-down technology, to elucidate the precise molecular events contributing to these alterations in gene expression.

GO enrichment analysis has been widely used to investigate the coherent functional signal among multiple genes. For these unique peaks-containing genes in the UVR sample, we found that some of them were highly involved in response to oxidative stress and autophagy processes [25], which have been shown to play an important role in photoaging. Moreover, in relation to genes exhibiting disparities in both m^{6}A levels and expression levels, the outcomes of GO enrichment analysis evinced a multiplicity of biological processes closely associated with extracellular matrix and collagen metabolism within the hyper-down fraction of genes. Conversely, other portions of genes failed to manifest any processes associated with photoaging. These results suggest that m^{6}A modifications are involved in multiple aspects of the photoaging mechanism, not only MFAP4 in this study. Therefore, more investigations on other genes with altered m^{6}A modifications and associated with photoaging are needed in the future.

Conclusions

In summary, our study has illustrated the crucial role of KIAA1429 in collagen metabolism and an activated KIAA1429-mediated m^{6}A machinery in photoaging. KIAA1429 upregulation contributes to the m^{6}A

modification of MFAP4 followed by expression reduction via an epigenetic manner. Our results enrich that the functional value of KIAA1429 may serve as an emerging epitranscriptomic mechanism to regulate collagen metabolism in photoaging. We anticipate that these findings provide a new theoretical foundation for the prevention of photoaging.

Methods

Mice and UVR irradiation

A total of 30, six-week-old male C57/BL6 mice were purchased from Orient Bio Inc. (Beijing, China), and they were fed according to standard procedures. After one week of adaptive feeding, the mice were randomly divided into two groups, namely, the control group ($n=7$) and the UVR group ($n=7$). All mice were shaved once a week. The UVR mice were irradiated with a mixed source of UVA (315 nm ~ 400nm, 0.60 mW/cm^2) and UVB (290nm ~ 315nm, 3.5 mW/cm2) ray every other day for 12 weeks. The initial irradiation time was 15 min for the first week base on the minimal erythema dose (MED), followed by a graduated increase until it reached 80 min. The total irradiated dose was approximately 151 J/cm^2 for UVA and 23 J/cm^2 for UVB, respectively. All animal work has been approved by the Seventh Medical Center of PLA General Hospital Animal Care and Use Committee.

Histological analysis

HE and Masson were performed as previously described [26]. Briefly, after deparaffinization and rehydration, for HE staining, longitudinal sections of 5 μm were stained with hematoxylin solution for 1 min, then soaked in 1% acidic ethanol for 10 s followed by rinsing with distilled water. The sections were subsequently stained with eosin solution for 5 min, and then dehydrated in graded alcohol and cleared in xylene. For Masson staining, slices were stained with Weigert hematoxylin solution for 5 min, followed by rinsing with water for 10 min, and then stained with Masson Li chunhong acid fuchsin staining solution for 10 min. The slices were then processed with phosphomolybdic acid solution for about 3 min, followed by direct staining with Aniline Blue staining solution without washing for 5 min. Thereafter, the sections were treated with 0.2% glacial acetic acid solution, dehydrated, and sealed. Three sections from each group were mounted on slides and then observed and photographed under a light microscope.

Real time quantitative PCR (RT-qPCR) analysis

Total RNA was extracted from fresh skin tissues and cells with TRIzol reagent (Invitrogen, USA). Reverse transcribed to cDNA for PCR analyses was synthesized with a PrimeScriptTM RT Reagent Kit with gDNA Eraser (Perfect Real Time) (Takara, Japan), and qPCR was performed using Power SYBR Green PCR Master Mix (Applied Biosystems, USA) according to the manufacturer's protocol. Tubulin was used as an internal reference gene and the $2^{-\triangle\triangle CT}$ method was used to calculate the relative expression of the target RNA. All the primer sequences were synthesized by Tsingke Biotech (Beijing, China). (Additional file 4: Table S3). Each experiment was repeated in triplicate.

Enzyme-linked immunosorbent assay (ELISA)

SOD, MDA and Hyp levels in the skin tissues lysates after UVR irradiation were determined using an ELISA kit (Mouse SOD, Mouse MDA and Mouse Hyp) (Beyotime, China) according to the manufacturer's instructions. A microplate reader (Thermo Fisher Scientific, Carlsbad, CA, USA) was used to calculated the concentrations of SOD, MDA and Hyp by measuring the absorbance of the samples at 450 nm. Each experiment was repeated in triplicate.

Western blotting

Western blot was performed to analyze the expression of MMP1, TGF-bRII, KIAA1429 and MFAP4 in HDFs or skin tissues. Cells and tissues were lysed in PIPA buffer containing protease inhibitor and phosphatase inhibitor, followed by dispersed ultrasonically and the concentration of protein was determined with a BCA assay kit (Thermo Fisher Scientific, USA). 40 μg/porin was separated from SDS-PAGE gel, and then the sample was transferred onto polyvinylidene fluoride (PVDF) membranes. After that, the membranes were blocked with blocking solution and incubated with primary antibodies against MMP1 (1:800, Proteintech, USA), TGF-bRII (1:1000, Proteintech, USA), KIAA1429 (1:500, Proteintech, USA), MFAP4 (1:500, Proteintech, USA), and Tubulin (1:2000, Proteintech, USA) overnight, respectively. Finally, the membranes were rinsed with Tris-buffered saline containing Tween 20 (TBST) and incubated with horseradish peroxidase (HRP)-conjugated goat anti-rabbit IgG (1:5000, Proteintech, USA) for 2 h. Bands were quantified by ImageJ software (version 1.8.0).

m^{6}A dot blot assay

The m^{6}A dot assay was basically performed as previously described with modifications [27]. Total RNA was extracted as described above and purified with Dynabeads mRNA Purification Kit (Thermo Scientific). Serial-diluted RNA samples were denatured at 95 ℃ for 3 min followed by being chilled on ice immediately. Thereafter, an equal volume of RNA was loaded onto the Hybond-N + membrane (GE Healthcare, USA), crosslinked with UV light, wash with TBST, and stained with Methylene

blue (Solarbio Biotech, China) as a quantitative control for total RNA. Whereafter, it was blocked with 5% milk in TBST for 2 h and incubated with Rabbit anti-m^{6}A antibody (1:1000, Abcam, United Kingdom) at 4 ℃ overnight. Finally, the HRP-linked secondary anti-rabbit IgG antibody (1:5000, CST, USA) was used to visualize the dot blot with enhanced chemiluminescence. The dots were quantified using ImageJ software (version 1.8.0). Each experiment was repeated in triplicate.

Immunohistochemical (IHC) Staining

IHC staining of skin tissues was performed following routine steps. Briefly, after deparaffinization and rehydration, sections were processed by blocking endogenous peroxidase activities, retrieving antigen and reducing nonspecific binding, followed by incubating with primary antibodies against KIAA1429 (1:500, Proteintech, USA), secondary antibodies and staining agent. IHC scores were calculated by multiplying the staining intensity score (0, 1, 2 or 3 indicated negative, weakly positive, positive or strongly positive, respectively) and positive rate score (0, 1, 2, 3 or 4 implied 0%, 1–25%, 26–50%, 51–75% or 76–100% of the positive area, respectively) by two pathologists independently.

MeRIP sequencing and RNA sequencing

Total RNA was extracted using TRIzol Reagent (Invitrogen, USA) and qualified by a NanoDrop™ 2000 (Thermo Fisher Scientific, USA) instrument. 20 μg total RNAs were used for rRNA removal using the KC-Digital™ Total RNA-seq Library Prep Kit (Human/Mouse/Rat) (Catalog NO. DLR08702, Wuhan Seqhealth Co., Ltd. China) followed by fragmented into 100–200 nt. 10% of the RNA fragment was utilized as "input" and the remainder was enriched by immunoprecipitation with anti-m^{6}A specific antibody (Synaptic Systems, 202,203). RNA-seq libraries of m^{6}A antibody-enriched RNAs and input RNAs were constructed by KC-Digital Stranded mRNA Library Prep Kit for Illumina® (Wuhan Seqhealth Co., Ltd. China) following the manufacturer's instruction. The kit eliminates duplication bias in PCR and sequencing steps, by using unique molecular identifier (UMI) of 8 random bases to label the pre-amplified cDNA molecules. The library products corresponding to 200–500 bps were enriched, quantified and finally sequenced on DNBSEQ-T7 sequencer (MGI Tech Co., Ltd. China) with PE150 model.

Data analysis

Raw sequencing data were filtered with Trimmomatic software and treated with in-house scripts to eliminate duplication bias introduced in library preparation and sequencing. After that, the de-duplicated consensus sequences of IP and input were mapped to the mice reference genome GRCm38 using STAR software (version 2.5.3a). For MeRIP-seq, the analysis of m^{6}A peak calling, annotation and distribution were performed with exomePeak (Version 3.8), bedtools (Version 2.25.0) and deepTools (version 2.4.1), respectively. Differentiated m^{6}A peaks were identified by a python script using the fisher test, with significance determined as FDR < 0.05. Homer (version 4.10) was used to identify sequence motifs enriched in the m^{6}A peak region. For RNA-seq, featureCounts (Subread-1.5.1; Bioconductor) was used to calculate the number of reads mapped to the exonic region of each gene, and then RPKMs were calculated. The edgeR package (version 3.12.1) was used for differentially expressed genes (DEGs) analysis and the screening criteria were set with a p-value < 0.05 and | Fold Change (FC) |≥ 2. Gene ontology (GO) enrichment and Kyoto encyclopedia of genes and genomes (KEGG) pathway analysis were performed to investigate the probable function of DEGs and differentially m^{6}A methylated genes (DMMGs) [28, 29].

MeRIP-qPCR validation

Utilizing a reported methodology, the analysis of MeRIP-qPCR was performed. Briefly, mRNA underwent fragmentation through the use of m^{6}A RNA methylation fragment enrichment kit (IVDSHOW, China).

A minute fraction of the fragmented RNA was reserved as input RNA. Following fragmentation, the RNA was subjected to immunoprecipitation with anti-m^{6}A antibody coupled to Affinity Beads through the use of MeRIP Kit (IVDSHOW, China) at room temperature for 100 min. Washed three times with Protein Digestion Buffer and the Wash Buffer. 20μl Protein Digestion Solution was added and incubated at 55° C for 15 min. After washed by 90% ethanol, the beads were resuspended in Elution Buffer and incubated at room temperature for 5 min to release RNA from the beads. The beads were caught by placing the tube in a magnetic frame. Transferred the sample to new tubes and stored at -80°C. The determination of m^{6}A enrichment was assessed by means of qPCR analysis. The primer sequences utilized in the procedure can be found in Additional file 5: Table S4.

Cell culture and UVR irradiation

HDFs (ATCC No.PCS-201–012) were purchased from Bena Culture Collection (Peking, China) and inoculated with DMEM medium containing 10% fetal bovine serum (Gibco, USA), 1% penicillin/streptomycin (Gibco, USA), and cultured at 37 °C in a 5% CO_2 incubator. UVR irradiation was performed when the cell density reached 90%. Briefly, the HDFs were washed twice with PBS and exposed to UVR for 10 s to reach a total dose of

approximately 5 J/cm^2 for UVA and 23 mJ/cm^2 for UVB, respectively. After UVR irradiation, cells were washed with PBS again followed by incubated in serum-free DMEM medium for 24 h. The cell lysate was collected for quantitative ELISA and WB as shown above. All of the cell experiments were performed in triplicate.

RNA interference

The siRNA directed against KIAA1429, MFAP4 and negative control (si-NC) were designed and synthesized by GenePharma Company (Shanghai, China). The sequences were as follows: si-NC (UUCUCCGAACGUGUCACGUTT),

si-KIAA1429 (si-KIAA1429-1, CCAUCAUCUUUAGACCUAATT; si-KIAA1429-2, GGAAGAACCAAGACUACUAAA) and si-MFAP4 (si-MFAP4-1, AAUCUCUUCUGGAAAACCGUC, si-MFAP4-2 CGACAUCTAUGCCCA). siRNA was transient transfected into HDFs using Lipofectamine 2000 (Invitrogen, CA, USA) according with the standard protocol. After 48 h of transfection, the HDFs photoaging model was constructed as described above.

Immunofluorescence

The HDFs were cultured on glass coverslips, then were fixed and permeabilized in 4% PFA with 0.1% Triton X and blocked with 5% Bovine Serum Albumin (BSA), before staining with the primary antibodies for MFAP4 (Proteintech, 1: 200) and COL1A2 (with SF555, Huaxing biotech, 1: 200). After washing, the cells were incubated with secondary antibodies conjugated with Alexa 488 (Proteintech, 1:400). The coverslips were mounted with antifade Mounting Medium with DAPI and Propidium Iodide (Beyotime) and visualized using an EVOS FL Auto microscope (Thermo Fisher Scientific).

Statistical analysis

Data were expressed as the mean ± SD and analyzed by SPSS 24.0 (NY: IBM Corp, USA). Pairwise comparisons were performed using unpaired t-test or one-way analysis of variance (ANOVA), and the level of statistically significant was considered as $^{*}P<0.05$; $^{**}P<0.01$; $^{***}P<0.001$. GraphPad Prism 7.0 was performed to generate graphs (GraphPad Software Inc, USA).

Abbreviations

m^{6}A	N6-Methyladenosine
RT-qPCR	Real-time quantitative PCR
IHC	Immunohistochemical
MeRIP-seq	Methylated RNA immunoprecipitation sequencing)
HDFs	Human dermal fibroblasts
NER	Noncanonical nucleotide excision repair
GGR	Global genome repair
SOD	Superoxide dismutase
Hyp	Hydroxyproline
MDA	Malondialdehyde
TGF-βRII	Transforming growth factor-beta receptor 2
MMP-1	Matrix metalloproteinase 1
HE	Hematoxylin–eosin
ANOVA	One-way analysis of variance
siRNA	Small interfering RNAs
CLIP	Crosslinking and immunoprecipitation

Supplementary Information

The online version contains supplementary material available at https://doi.org/10.1186/s12915-024-01976-0.

Additional file 1: Supplementary Table 1- Differentially m6A methylated genes in control vs. UVR-induced samples.

Additional file 2: Supplementary Table 2- Differentially expressed genes in control vs. UVR-induced samples

Additional file 3: Supplementary Figure 1-3. Figure S1. The top 20 GO biological processes enrichments of genes from the hyper-up part. Figure S2. The top 20 GO biological processes enrichments of genes from the hypo-up part. Figure S3. The top 20 GO biological processes enrichments of genes from the hypo-down part.

Additional file 4: Supplementary Table 3- Primers used for select genes by RT-qPCR.

Additional file 5: Supplementary Table 4- Primers used for select genes by meRIP-qPCR.

Additional file 6. Images of uncropped gels.

Acknowledgements

None

Authors' contributions

Y.L., J.L., and C.W. contributed equally to this work and share first authorship. Y.L., J.L., and C.W. conceived and designed the experiments. Y.L., J.L., C.W., J.L., K.L., K.T., Y.T., X.S., Z.Z., Y.Z., W.L., and Y.J. performed the experiments. Y.L., J.L., C.W., J.L., K.L., K.T., Y.T., X.S., Z.Z., Y.Z., W.L., and Y.J. analyzed the data. Y.L., J.L., C.W., J.L., K.L., K.T., Y.T., X.S., Z.Z., Y.Z., W.L., and Y.J. contributed reagents/materials/analysis tools. Y.L., J.L., C.W., J.L., K.L., K.T., Y.T., X.S., Z.Z., Y.Z., W.L., and Y.J. wrote the paper. R.Y. and M.Z. contributed equally to this work and share senior authorship. R.Y. and M.Z. supervised the project. Y.D.T. and R.Y. provided critical feedback and guidance.
All authors read and approved the final manuscript.

Funding

This work was supported by the National Natural Science Foundation of China (NO. 82002120), the National Science Foundation of Chongqing, China (NO. cstc2021jcyj-msxmX0140) and Chongqing Doctoral "Through Train" Research Project (CSTB2022BSXM-JCX0021).

Availability of data and materials

All data generated or analysed during this study are included in this published article, its supplementary information files and publicly available repositories (GEO: GSE268348). Raw data from Figures were deposited on Mendeley at https://data.mendeley.com/datasets/h3r6bthfx2/1

Declarations

Ethics approval and consent to participate

All animal work has been approved by the Seventh Medical Center of PLA General Hospital Animal Care and Use Committee (SYXK 2022–0018).

Consent for publication

Authors consent for publication.

Competing interests

The authors declare that they have no competing interests.

Author details
[1]Medical School of Chinese People's Liberation Army, Beijing 100039, China. [2]Department of Dermatology, the Seventh Medical Center of Chinese PLA General Hospital, Beijing 100010, China. [3]Department of Dermatology, Southwest Hospital, Army Medical University, Chongqing 400038, China. [4]Bioinformatics Center of AMMS, Beijing 100063, China. [5]Biomedical Treatment Center, the Seventh Medical Center of Chinese, PLA General Hospital, Beijing 100010, China. [6]Department of Pediatric Urology, the Seventh Medical Center of Chinese, PLA General Hospital, Beijing 100010, China. [7]Shandong University of Traditional Chinese Medicine, ShanDong 250355, China. [8]Tianjin University of Traditional Chinese Medicine, Poyanghu Road, Tianjin 301617, China.

Received: 13 July 2023 Accepted: 7 August 2024
Published online: 11 September 2024

References

1. Kohl E, Steinbauer J, Landthaler M, Szeimies RM. Skin ageing. J Eur Acad Dermatol Venereol. 2011;25(8):873–84.
2. Fitsiou E, Pulido T, Campisi J, Alimirah F, Demaria M. Cellular Senescence and the Senescence-Associated Secretory Phenotype as Drivers of Skin Photoaging. J Invest Dermatol. 2021;141(4S):1119–26.
3. Meyer KD, Saletore Y, Zumbo P, Elemento O, Mason CE, Jaffrey SR. Comprehensive analysis of mRNA methylation reveals enrichment in 3' UTRs and near stop codons. Cell. 2012;149(7):1635–46.
4. Zaccara S, Ries RJ, Jaffrey SR. Reading, writing and erasing mRNA methylation. Nat Rev Mol Cell Biol. 2019;20(10):608–24.
5. Jiang X, Liu B, Nie Z, Duan L, Xiong Q, Jin Z, et al. The role of m6A modification in the biological functions and diseases. Signal Transduct Target Ther. 2021;6(1):74.
6. Xiang Y, Laurent B, Hsu C-H, Nachtergaele S, Lu Z, Sheng W, et al. RNA mA methylation regulates the ultraviolet-induced DNA damage response. Nature. 2017;543(7646):573–6.
7. Yang Z, Yang S, Cui Y-H, Wei J, Shah P, Park G, et al. METTL14 facilitates global genome repair and suppresses skin tumorigenesis. Proc Natl Acad Sci U S A. 2021;118(35):e2025948118.
8. Liu S, You L, Zhao Y, Chang X. Hawthorn Polyphenol Extract Inhibits UVB-Induced Skin Photoaging by Regulating MMP Expression and Type I Procollagen Production in Mice. J Agric Food Chem. 2018;66(32):8537–46.
9. Nagarajan A, Janostiak R, Wajapeyee N. Dot Blot Analysis for Measuring Global N-Methyladenosine Modification of RNA. Methods In Molecular Biology (Clifton, NJ). 2019;1870:263–71.
10. Resource TGO. 20 years and still GOing strong. Nucleic Acids Res. 2019;47(D1):D330–8.
11. Kanehisa M, Goto S. KEGG: kyoto encyclopedia of genes and genomes. Nucleic Acids Res. 2000;28(1):27–30.
12. Shi H, Wei J, He C. Where, When, and How: Context-Dependent Functions of RNA Methylation Writers, Readers, and Erasers. Mol Cell. 2019;74(4):640–50.
13. Dominissini D, Moshitch-Moshkovitz S, Schwartz S, Salmon-Divon M, Ungar L, Osenberg S, et al. Topology of the human and mouse m6A RNA methylomes revealed by m6A-seq. Nature. 2012;485(7397):201–6.
14. Ma J, Teng Y, Huang Y, Tao X, Fan Y. Autophagy plays an essential role in ultraviolet radiation-driven skin photoaging. Front Pharmacol. 2022;13:864331.
15. Birch-Machin MA, Bowman A. Oxidative stress and ageing. Br J Dermatol. 2016;175(Suppl 2):26–9.
16. Kasamatsu S, Hachiya A, Fujimura T, Sriwiriyanont P, Haketa K, Visscher MO, et al. Essential role of microfibrillar-associated protein 4 in human cutaneous homeostasis and in its photoprotection. Sci Rep. 2011;1:164.
17. Pan Z, Yang K, Wang H, Xiao Y, Zhang M, Yu X, et al. MFAP4 deficiency alleviates renal fibrosis through inhibition of NF-κB and TGF-β/Smad signaling pathways. FASEB J. 2020;34(11):14250–63.
18. Sen P, Shah PP, Nativio R, Berger SL. Epigenetic Mechanisms of Longevity and Aging. Cell. 2016;166(4):822–39.
19. Ouyang M, Fang J, Wang M, Huang X, Lan J, Qu Y, et al. Advanced glycation end products alter the mA-modified RNA profiles in human dermal fibroblasts. Epigenomics. 2022;14(8):431–49.
20. Zhao Q, Chen Y, Qu L. Combined Transcriptomic and Proteomic Analyses Reveal the Different Responses to UVA and UVB Radiation in Human Keratinocytes. Photochem Photobiol. 2023;99(1):137–52.
21. Schwartz S, Mumbach MR, Jovanovic M, Wang T, Maciag K, Bushkin GG, et al. Perturbation of m6A writers reveals two distinct classes of mRNA methylation at internal and 5' sites. Cell Rep. 2014;8(1):284–96.
22. Yue Y, Liu J, Cui X, Cao J, Luo G, Zhang Z, et al. VIRMA mediates preferential mA mRNA methylation in 3'UTR and near stop codon and associates with alternative polyadenylation. Cell Discov. 2018;4:10.
23. Zhang X, Li MJ, Xia L, Zhang H. The biological function of m6A methyltransferase KIAA1429 and its role in human disease. PeerJ. 2022;10:e14334.
24. Zhu W, Wang J-Z, Wei J-F, Lu C. Role of m6A methyltransferase component VIRMA in multiple human cancers (Review). Cancer Cell Int. 2021;21(1):172.
25. Wu F, Zhang L, Lai C, Peng X, Yu S, Zhou C, et al. Dynamic Alteration Profile and New Role of RNA m6A Methylation in Replicative and HO-Induced Premature Senescence of Human Embryonic Lung Fibroblasts. Int J Mol Sci. 2022;23(16):9271.
26. Hirano E, Fujimoto N, Tajima S, Akiyama M, Ishibashi A, Kobayashi R, et al. Expression of 36-kDa microfibril-associated glycoprotein (MAGP-36) in human keratinocytes and its localization in skin. J Dermatol Sci. 2002;28(1):60–7.
27. Pilecki B, Holm AT, Schlosser A, Moeller JB, Wohl AP, Zuk AV, et al. Characterization of Microfibrillar-associated Protein 4 (MFAP4) as a Tropoelastin- and Fibrillin-binding Protein Involved in Elastic Fiber Formation. J Biol Chem. 2016;291(3):1103–14.
28. Kanaan R, Medlej-Hashim M, Jounblat R, Pilecki B, Sorensen GL. Microfibrillar-associated protein 4 in health and disease. Matrix Biol. 2022;111:1–25.
29. Wang M, Charareh P, Lei X, Zhong JL. Autophagy: Multiple Mechanisms to Protect Skin from Ultraviolet Radiation-Driven Photoaging. Oxid Med Cell Longev. 2019;2019:8135985.

Publisher's Note